nature catalysis

Article

https://doi.org/10.1038/s41929-026-01524-9

A high-flux membrane electrode assembly for CO_2 electroreduction to 4.5 M formate with over 8,000 h stability

Received: 21 January 2025

Accepted: 11 March 2026

Published online: 03 April 2026

Check for updates

Jing-Jing Li[1], Hong-Juan Wang[1], Chao Zhang[1], Yu Li[1], Jiqing Jiao[1], Lin-Lin Wang[1], Cuo Wu[1], Di-Chang Zhong[1], Zhen-Yu Wu[2], Zi-You Yu[1] ✉ & Tong-Bu Lu[1] ✉

The direct electroreduction of CO_2 at an electrolyte-free cathode to generate liquid chemical products with high concentration, selectivity and stability is highly desired, yet extremely challenging, and such systems are lacking. Here we report a high-flux membrane electrode assembly design that uses core–shell structural Cu/Bi nanowires grown on three-dimensional Cu foam with a mean pore size of 190 μm (3D-Cu/Bi) as the cathode. Benefiting from the abundant active sites and high permeability of 3D-Cu/Bi, the catholyte-free membrane electrode assembly-based electrolyser can directly convert CO_2 into formate with a high concentration of 4.5 M and maintain a high Faradaic efficiency of ~90% for 8,000 h at 200 mA cm^{-2}. We further demonstrate the continuous production of concentrated formate solution with a scaled-up 100 cm^2 electrolyser at 20 A for over 2,000 h.

The synthesis of value-added chemicals via the electrocatalytic carbon dioxide reduction reaction (CO_2RR) using renewable electricity is a promising approach for achieving carbon neutrality[1–5]. Over the past decade, a variety of catalysts and devices have been developed that exhibit high current density and selectivity for the generation of diverse CO_2RR products[6–8]. Among these products, carbon monoxide and formate are considered to be the most commercializable products. Recent techno-economic analyses[9–11] have determined the industrially relevant activity and the Faradaic efficiency (FE) to be >200 mA cm^{-2} and >90%, respectively. In particular, formate is a very attractive CO_2RR product, on account of its easy transportation and storage and wide applications in the textile, leather and pharmaceutical industries[12–14]. However, the as-obtained formate is usually mixed and diluted with electrolytes in conventional H-type and flow-cell reactors, leading to a very-low-concentration formate solution (typically <0.1 M)[15]. It thus requires energy-intensive downstream separation and concentration processes[16,17]. The direct production of high-concentration formate via the electrocatalytic CO_2RR is therefore highly desired for practical applications, although it remains challenging.

To address this tough issue, Wang and colleagues reported a CO_2RR electrolyser based on a three-layer membrane architecture, where cathodically produced $HCOO^-$ ions passing through an anion exchange membrane (AEM) and anodically produced H^+ ions passing through a cation exchange membrane (CEM) are combined in a porous solid-state electrolyte (PSE) layer to form pure formic acid with concentrations of up to 12 M (ref. 16). However, some problems persist for this AEM/PSE/CEM-based CO_2 electrolyser[17]. For example, the high concentration of formic acid can decrease its selectivity (12.1 M formic acid with 40% FE versus 1.8 M formic acid with 80% FE), mainly owing to the shift in thermodynamic equilibrium against the CO_2RR with an increased product concentration. Moreover, this CO_2 electrolyser with three-layer membranes has a high operating voltage and a high electrolyser cost, limiting its practical application[15–20].

Compared with the above-described multilayer architecture, a zero-gap membrane electrode assembly (MEA) electrolyser using

[1]MOE International Joint Laboratory of Materials Microstructure, Institute for New Energy Materials and Low Carbon Technologies, School of Materials Science & Engineering, Tianjin University of Technology, Tianjin, China. [2]Department of Chemistry, Institute of Innovative Material, Guangdong Provincial Key Laboratory of Sustainable Biomimetic Materials and Green Energy, Southern University of Science and Technology, Shenzhen, China. ✉e-mail: yuziyou@email.tjut.edu.cn; lutongbu@tjut.edu.cn

https://doi.org/10.1038/s41929-026-01524-9

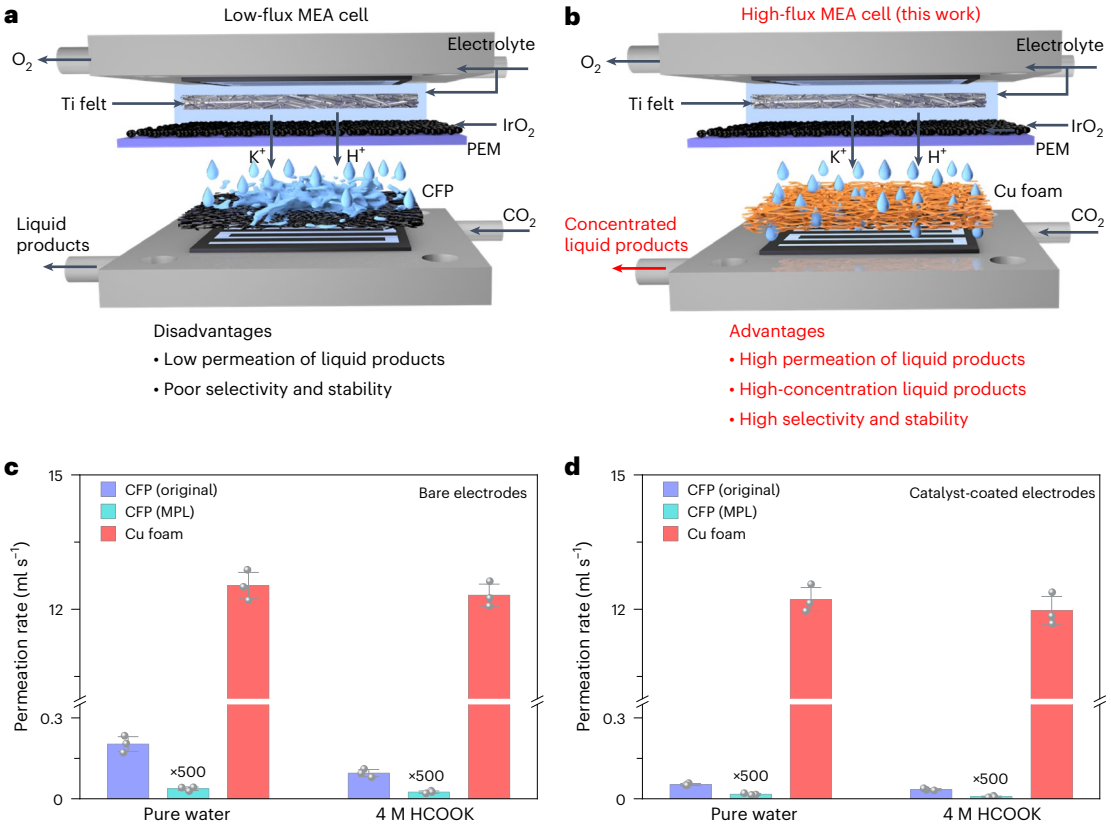

Fig. 1 | The high-flux MEA design. a, Low-flux MEA cell. PEM, proton exchange membrane. **b**, The high-flux MEA cell of this work. **c**,**d**, Permeation rates for the bare electrodes (**c**) and the catalyst-coated electrodes (**d**) in pure water and 4 M formate solution (HCOOK). The data represent the mean values from three independent measurements, and the error bars indicate the standard deviation.

a layer of AEM or CEM has a simpler configuration and lower ohmic losses (Fig. 1a,b)[21–24]. The direct supply of dry or humidified CO_2 gas without adding a catholyte in an MEA electrolyser is a very promising route for producing concentrated formic acid or formate[17,19,25–27]. However, the continuous generation of high-concentration formate via an MEA-based CO_2 electrolyser at industrially relevant current densities for more than 100 h has rarely been reported[19,25–28].

Although carbon fibre paper (CFP) is commonly used as the gas diffusion electrode in MEA-based CO_2 electrolysers, it remains an open question whether CFP is ideal for such systems, because the generated liquid products do not transport quickly through a CFP electrode and easily accumulate on the CFP surface (Fig. 1a). The accumulated liquid products can block the channels for CO_2 transport and further worsen the infiltration through the electrode, both of which lead to a hampered activity and poor stability. The main challenge is how to transport the concentrated liquid products rapidly away from the cathode surface.

In this Article we propose replacing the CFP with high-flux Cu foam as the catalyst-supporting electrode, where this Cu foam has rich macropores to allow the fast permeation of liquid products (Fig. 1b). On the basis of this concept, we constructed an active Cu/Bi core–shell heterostructure catalyst on a three-dimensional Cu foam surface (3D-Cu/Bi), which displays an outstanding catalytic performance for CO_2RR-to-formate conversion. When fed with dry CO_2 gas without adding any catholyte, the assembled MEA-based CO_2 electrolyser using 3D-Cu/Bi as the cathode can continuously produce 4.5 M formate with a Faradaic efficiency for the production of formate ($FE_{formate}$) of ~90% for more than 8,000 h at 200 mA cm^{-2}, representing one of the most durable CO_2 electrolysers for the production of high-concentration formate. We also demonstrate the scalability of our design as a larger-sized electrolyser with an active area of 100 cm^2, which achieved a high formate production rate of 318 mmol h^{-1} at 20 A for 2,000 h.

Results

The choice of high-flux Cu foam substrate

Two types of common CFP, including the original CFP and CFP coated with a microporous layer (MPL), were used for comparison (Supplementary Fig. 1). The Cu foam substrate was chosen as a high-flux electrode because of its robust 3D framework, excellent electrical conductivity and rich pores that have a size of several hundred micrometres (Supplementary Fig. 1). We first used a simplified device to simulate the permeation processes for different electrode substrates with the same geometric area (Supplementary Figs. 2 and 3). For pure water, the original CFP has a permeation rate of 0.2 ml s^{-1}, which decreases to ~0.08 µl s^{-1} for the MPL-coated CFP (Fig. 1c), indicating a notable lowered permeability after deposition of the hydrophobic MPL (Supplementary Fig. 4). By contrast, pure water could rapidly permeate the bare Cu foam with a rate as high as 12.5 ml s^{-1}, 60 times faster than that of the original CFP. The Cu foam and uncoated CFP display similar water contact angles (Supplementary Fig. 4), indicating that the fast liquid permeation through the Cu foam is due to its large pore size rather than the hydrophobicity. Similar results have been observed in concentrated formate solution, such as 4 M potassium formate (Fig. 1c). Even when coated with commercial Bi powder (a common catalyst used for the CO_2RR-to-formate conversion), the Cu foam electrode has a permeation rate that is still overwhelmingly higher than the two types of CFP in both pure water and concentrated formate solution (Fig. 1d). In addition, after the permeation tests, severe precipitation of the formate salt was observed for the CFP electrode, although not for the Cu foam (Supplementary Fig. 5). These results indicate that the Cu foam can be used as an excellent substrate candidate to replace CFP for the fast permeation of concentrated liquid products in MEA-based CO_2 electrolysers (Fig. 1b).

https://doi.org/10.1038/s41929-026-01524-9

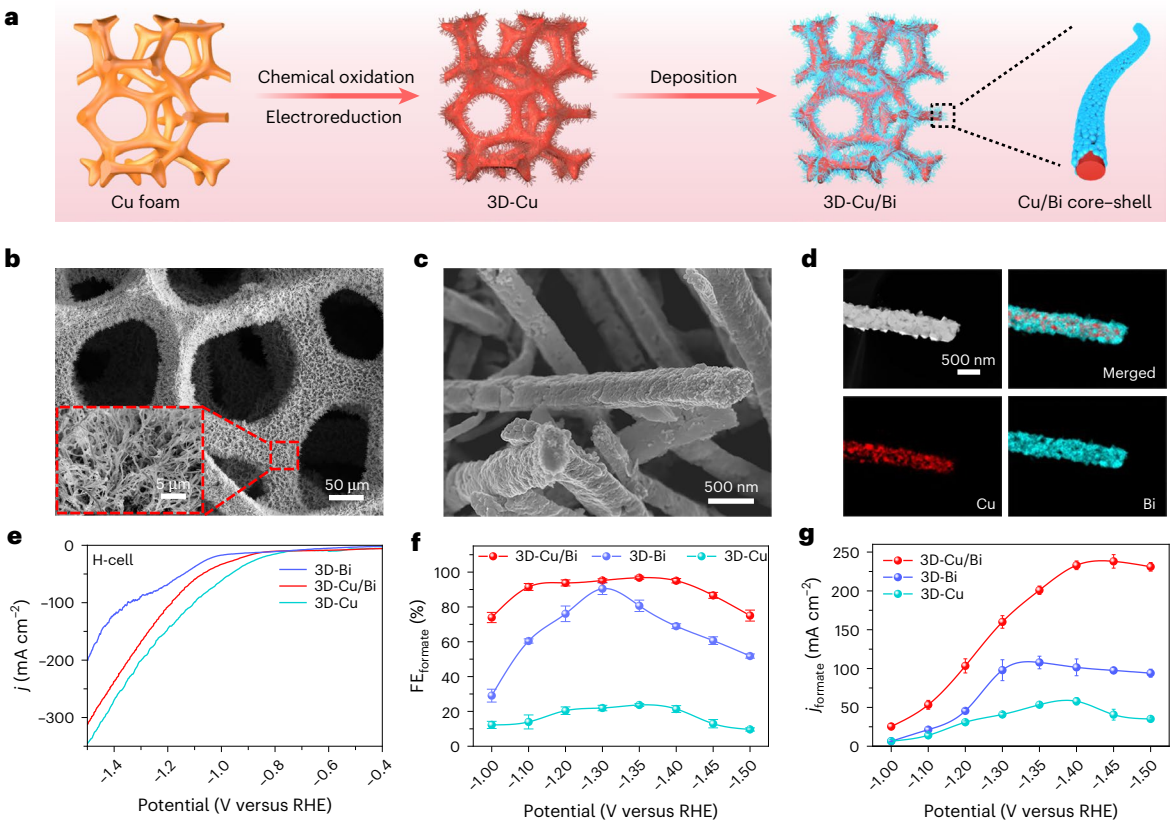

Fig. 2 | Preparation, characterization and CO_2RR performance of the 3D-Cu/Bi catalyst. a, Schematic of the preparation of the 3D-Cu/Bi catalyst. **b**,**c**, Scanning electron microscopy (SEM) images of the 3D-Cu/Bi catalyst at lower (**b**) and higher (**c**) resolution. **d**, EDX elemental mapping images of the 3D-Cu/Bi catalyst. **e**–**g**, Linear sweep voltammetry curves (**e**), formate FE curves (**f**) and formate partial current densities (**g**) for the different catalysts in an H-type cell with CO_2-saturated 0.5 M K_2SO_4 and 3 mM H_2SO_4 as the electrolyte. In **f** and **g**, the data represent the mean values from three independent measurements, and the error bars indicate the standard deviation.

Synthesis and characterization of catalysts

We selected Bi as the catalyst due to its high selectivity for CO_2RR to formate, and we anticipated that construction of the Cu/Bi interface could further improve its performance. The direct growth of active catalysts on the 3D conductive Cu foam substrate can avoid the use of polymer binder and expose more active sites, thus lowering the electrode resistance and enhancing the catalytic performance. The synthesis of core–shell structural Cu/Bi nanowires on the 3D Cu foam framework is schematically illustrated in Fig. 2a (Methods). First, $Cu(OH)_2$ nanowires were grown in situ on the Cu foam framework, followed by annealing at 473 K in the air and electroreduction treatment to generate Cu nanowire arrays on the Cu foam (3D-Cu; Supplementary Fig. 6). The electrodeposition of Bi nanoparticles on the surface of the Cu nanowires for 60 min resulted in the formation of Cu/Bi core–shell nanowires on the Cu foam, with Cu/Bi nanowire diameters of 400–450 nm (Fig. 2b,c and Supplementary Fig. 7). X-ray diffraction patterns (Supplementary Fig. 7) showed the cubic Cu phase and the hexagonal Bi phase for the Cu/Bi catalyst, without any impurities or alloy phase. The high-resolution transmission electron microscopy image (Supplementary Fig. 8) reveals the distinct lattice planes from Cu(111) and Bi(012) at the Cu/Bi interface. Energy-dispersive X-ray (EDX) elemental mapping and line scanning (Fig. 2d and Supplementary Fig. 9, respectively) reveal the clear Cu/Bi core–shell structure of the 3D-Cu/Bi catalyst. Using EDX analysis (Supplementary Fig. 10) and inductively coupled plasma atomic emission spectroscopy, the molar ratio of Cu:Bi in the Cu/Bi core–shell nanowires was determined as ~1.2:1. We also prepared a series of 3D-Cu/Bi catalysts by adjusting the Bi electrodeposition time (20, 40 and 80 min). The results demonstrated that they all exhibit similar morphologies and structures with different Cu/Bi ratios (Supplementary Figs. 11–13). In addition, the Bi catalyst grown on Cu foam (3D-Bi) was also synthesized for comparison (Supplementary Fig. 14).

X-ray photoelectron spectroscopy and Cu Auger spectra show the primary Cu^0 and Bi^0 for the 3D-Cu/Bi catalyst (Supplementary Fig. 15). The small amounts of Bi^{3+} and Cu^+ species observed in 3D-Cu/Bi result from the inevitable surface oxidation when exposed to air[29,30]. Furthermore, CO_2 adsorption measurements showed that 3D-Cu/Bi catalyst has a threefold higher adsorption capability than that of 3D-Cu, indicating the strong surface enrichment of CO_2 on the Bi nanoparticles (Supplementary Fig. 16).

Synergistic effect on 3D-Cu/Bi for the CO_2RR to formate

We then assessed the electrocatalytic CO_2RR performance in an H-type cell using a three-electrode construction. To lower carbon loss in alkaline and neutral media[31,32], we used an acidic solution (0.5 M K_2SO_4 with 3 mM H_2SO_4) as the electrolyte (Supplementary Fig. 17). A comparison of the CO_2RR performance for 3D-Cu, 3D-Bi and 3D-Cu/Bi is shown in Fig. 2e–g and Supplementary Fig. 18. Although 3D-Cu has the highest current density (j), the main current contribution comes from the hydrogen evolution reaction. For the 3D-Bi catalyst, the CO_2RR to formate was markedly improved, reaching a maximum $FE_{formate}$ of 90% at −1.3 V and a partial current density towards formate ($j_{formate}$) of 100 mA cm^{-2}. Moreover, a maximum formate FE of 96.8% was achieved on the 3D-Cu/Bi catalyst, with H_2 production being largely suppressed to below 4%. Meanwhile, a high formate FE of >90% occurs over a wide potential region from around −1.1 to −1.4 V for the 3D-Cu/Bi catalyst, affording a partial formate current density of up to 233 mA cm^{-2} (Fig. 2g). We also optimized the Cu/Bi molar ratio by adjusting the Bi electrodeposition time (Supplementary Fig. 19).

https://doi.org/10.1038/s41929-026-01524-9

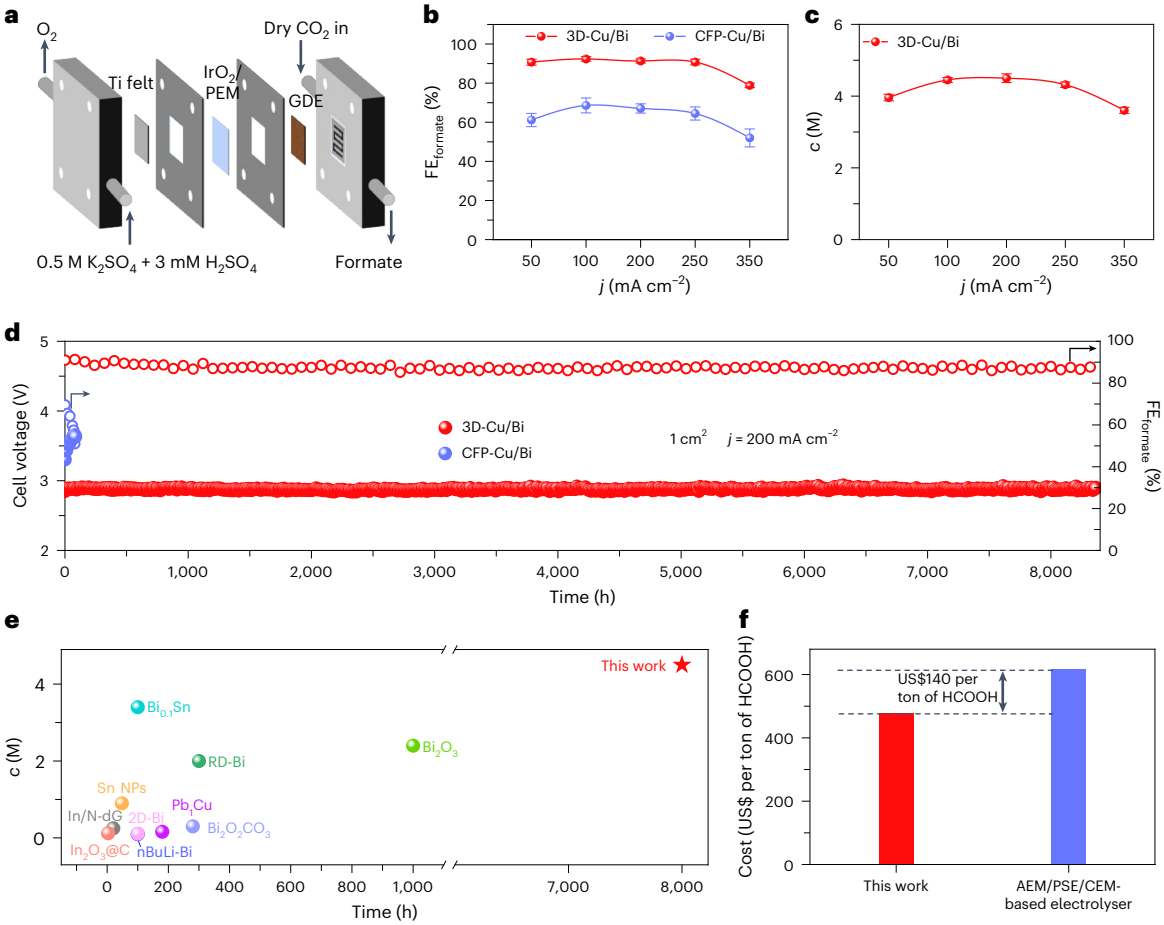

Fig. 3 | Electrocatalytic performance of the 1 cm² MEA-based electrolyser. **a**, Schematic of the MEA-based CO_2 electrolyser. GDE, gas diffusion electrode. **b**, Formate FE of the 3D-Cu/Bi and CFP-Cu/Bi catalysts. **c**, Formate concentration (*c*) of 3D-Cu/Bi at different current densities. **d**, Stability testing of 3D-Cu/Bi and CFP-Cu/Bi at a current density of 200 mA cm^{-2}. **e**, Comparison of the formate concentration and stability time of 3D-Cu/Bi with CO_2RR-to-formate catalysts in MEA-based and AEM/PSE/CEM-based CO_2 electrolysers reported in the literature. $Bi_{0.1}Sn$, $Bi_{0.1}Sn$ alloy; RD-Bi, rhombic dodecahedral Bi nanoparticles; Bi_2O_3, Bi_2O_3 nanoparticles; Sn NPs, Sn nanoparticles; Pb_1Cu, Pb-alloyed Cu catalyst; In/N-dG, In nanoparticle/chitosan-derived N-doped defective graphene catalyst; 2D-Bi, two-dimensional Bi catalyst; $Bi_2O_2CO_3$, $Bi_2O_2CO_3$ nanosheets; In_2O_3@C, carbon-confined indium oxide catalyst; *n*BuLi-Bi, *n*-BuLi-treated Bi catalyst. **f**, Techno-economic analysis for our MEA-based electrolyser and the best AEM/PSE/CEM-based electrolyser. In **b** and **c**, the data represent mean values from three independent measurements, and the error bars indicate the standard deviation.

Electrochemical impedance spectroscopy and Tafel slope analysis revealed that 3D-Cu/Bi has a low charge-transfer resistance and fast CO_2RR kinetics (Supplementary Figs. 20 and 21). Compared with previously documented catalysts[30,33–37], our 3D-Cu/Bi catalyst shows outstanding formate selectivity and a high partial current density in the H-type cell, and represents one of the most active CO_2RR-to-formate catalysts. Long-term stability testing reveals that the 3D-Cu/Bi catalyst can sustain a formate FE of >90% at ~150 mA cm^{-2} for over 100 h of continuous operation without any decay (Supplementary Fig. 22). Multiple characterization techniques showed that no obvious morphology and chemical-state changes were observed for the tested sample (Supplementary Fig. 23).

We then performed in situ ATR-IR (attenuated total reflectance infrared) spectroscopy to investigate the enhancement mechanism on the 3D-Cu/Bi catalyst. It should be noted that the adsorbed species *OCHO is widely considered to be the key and efficient intermediate for the electrocatalytic CO_2RR to formate[32,35,38–40]. Compared with 3D-Cu and 3D-Bi, the 3D-Cu/Bi catalyst exhibited stronger band intensities of the *OCHO intermediate and requires more positive potentials to form these bands (Supplementary Fig. 24), indicating the superior CO_2RR-to-formate activity for 3D-Cu/Bi. Density functional theory (DFT) calculations (Supplementary Figs. 25–27) further revealed that the Cu/Bi catalyst favours formation of the decisive *OCHO step with a low barrier energy[41,42]. These results demonstrate that the Cu/Bi interface catalyst can synergistically enhance the CO_2RR-to-formate performance.

Electrocatalytic performance of the MEA-based CO_2 electrolyser

As the formate product was mixed with vast amount of electrolytes (resulting in an extremely dilute formate solution) in the H-type cell, an MEA-based CO_2 electrolyser was constructed to obtain highly concentrated formate. Figure 3a and Supplementary Fig. 28 show the construction of the CO_2 electrolyser, with 3D-Cu/Bi as the cathode fed with dry CO_2 gas and the commercial IrO_2 catalyst as the anode fed with an acidic electrolyte, separated by a proton exchange membrane (Nafion 117). We optimized the Cu/Bi molar ratios of 3D-Cu/Bi catalysts and the anodic electrolytes in the MEA-based CO_2 electrolyser (Supplementary Fig. 29). For comparison, we also prepared a CFP-supported Cu/Bi (CFP-Cu/Bi) electrode using a similar synthesis method as for 3D-Cu/Bi except that the Cu precursor powder was coated onto the CFP with a Nafion binder (Supplementary Fig. 30). Benefiting from its high-flux properties, 3D-Cu/Bi showed a much higher current density and formate FE than the CFP-Cu/Bi electrode (Fig. 3b and Supplementary Fig. 31). As the cathode was fed with only dry CO_2 gas and no electrolyte was added, formate solution with a high

https://doi.org/10.1038/s41929-026-01524-9

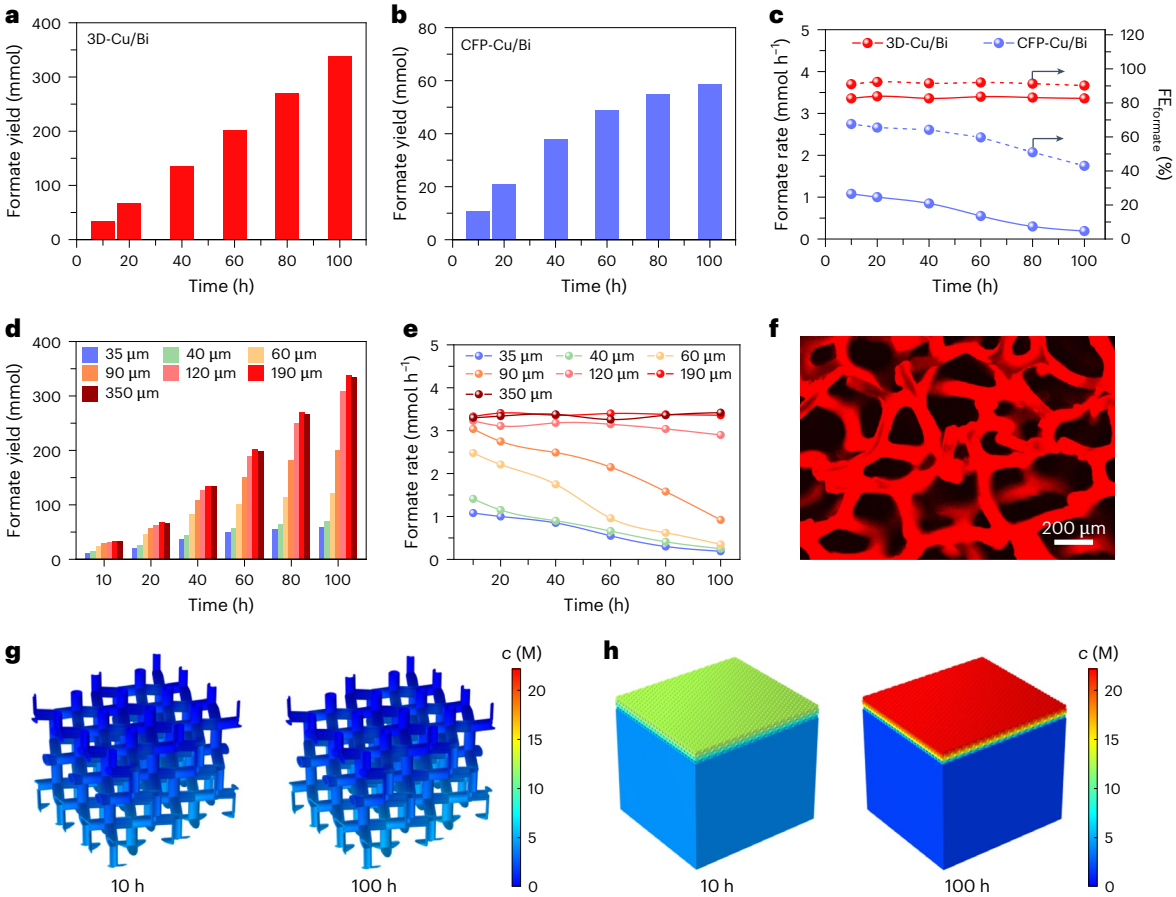

Fig. 4 | Origin of the high stability for the high-flux MEA design. a,**b**, Formate yield for (**a**) 3D-Cu/Bi and (**b**) CFP-Cu/Bi within the 100 h of electrolysis testing. **c**, Comparison of the formate production rate and formate FE for 3D-Cu/Bi and CFP-Cu/Bi. The formate production rate was calculated on the basis of the formate yield for a specific time period and not the accumulated yield. **d**,**e**, Formate yield (**d**) and formate production rate (**e**) for various electrodes within the 100 h of electrolysis testing. The catalyst substrates include CFP (35 μm) and Cu foam samples with different mean pores sizes (40, 60, 90, 120, 190 and 350 μm). **f**, Confocal fluorescence microscopy image of the rhodamine B-labelled 3D-Cu/Bi electrode after CO_2RR electrolysis. **g**,**h**, Concentration distribution of formate on the 3D-Cu/Bi surface (**g**) and on the CFP-Cu/Bi surface (**h**) after 10 and 100 h stability tests simulated via finite-element analysis.

concentration of 4.5 M was obtained at 200 mA cm^{-2} (Fig. 3c). Product analysis revealed that the final liquid product contains 91.1% HCOOK and 8.9% $KHCO_3$ (Supplementary Table 1), indicating a carbon loss of only ~8.9% in our system. Further increasing the acidity of the anolyte or decreasing the thickness of the membrane could reduce the bicarbonate content slightly, but this also compromised the formate FE and concentration (Supplementary Tables 1 and 2). When the CO_2 flow rate was decreased from 5 to 1.5 sccm (standard cubic centimetres per minute), 3D-Cu/Bi achieved a high single-pass carbon efficiency of 78.5% at 200 mA cm^{-2} (Supplementary Fig. 32).

Besides activity, the long-term stability of a system is an even more important performance metric for the practical application of CO_2 electrolysis. Our 3D-Cu/Bi electrode can continuously produce 4.5 M formate with an FE of ~90% at a cell voltage of 2.87 V for more than 8,000 h at 200 mA cm^{-2} without any deterioration (Fig. 3d and Supplementary Video 1). The 3D-Cu/Bi-based CO_2 electrolyser has negligible formate crossover (0.13%) from cathode to anode, much lower than that of the CFP-Cu/Bi-based CO_2 electrolyser (2.3%), due to the high-flux nature of the 3D-Cu/Bi electrode that is induced by the low accumulation of formate at the surface of Nafion 117, indicating the very low formate loss during the long-term stability test (Supplementary Fig. 33). However, CFP-Cu/Bi gradually lost its activity within <100 h. It should be noted that our 3D-Cu/Bi-based CO_2 electrolyser shows outstanding durability for the production of high-concentration formate at industrially relevant current density and FE values, and compares favourably with other CO_2 electrolysers reported in the literature (Fig. 3e and Supplementary Table 3)[15,16,18,20,25–27]. Considering that our electrolyser has a small cell voltage, a high formate concentration, a low electrolyser cost and an ultralong stability time, a techno-economic analysis demonstrated the feasibility of our MEA design compared with the best reported AEM/PSE/CEM-based electrolyser (Fig. 3f, Supplementary Fig. 34, Supplementary Tables 4 and 5 and Supplementary Notes 1 and 2). Moreover, our MEA electrolyser can achieve a high energy efficiency of 45.2% at 200 mA cm^{-2}, which is much higher than that of the best AEM/PSE/CEM-based electrolyser (26.5%; Supplementary Note 3). In addition, post-catalysis characterization shows that the structures of the 3D-Cu/Bi and proton exchange membrane are largely unchanged after CO_2RR electrolysis (Supplementary Figs. 35–38).

The origin of high stability for the high-flux MEA design

To uncover the origin of the excellent stability for our high-flux MEA design, we first carried out water contact angle measurements and found similar contact angles for 3D-Cu/Bi and CPF-Cu/Bi (Supplementary Fig. 39). After stability tests, we did not find any damage for both 3D-Cu/Bi and CPF-Cu/Bi electrodes, indicating their good mechanical strength. Therefore, we can exclude the influence of hydrophilic/hydrophobic behaviour and mechanical strength on the stability of the two electrodes. We further compared the formate production rate and formate FE for the 3D-Cu/Bi- and CFP-Cu/Bi-based electrolysers during the first 100 h of stability testing (Fig. 4a–c). The formate yield for the 3D-Cu/Bi electrolyser increased linearly with the reaction time, even for extended testing, thus achieving a stable formate

https://doi.org/10.1038/s41929-026-01524-9

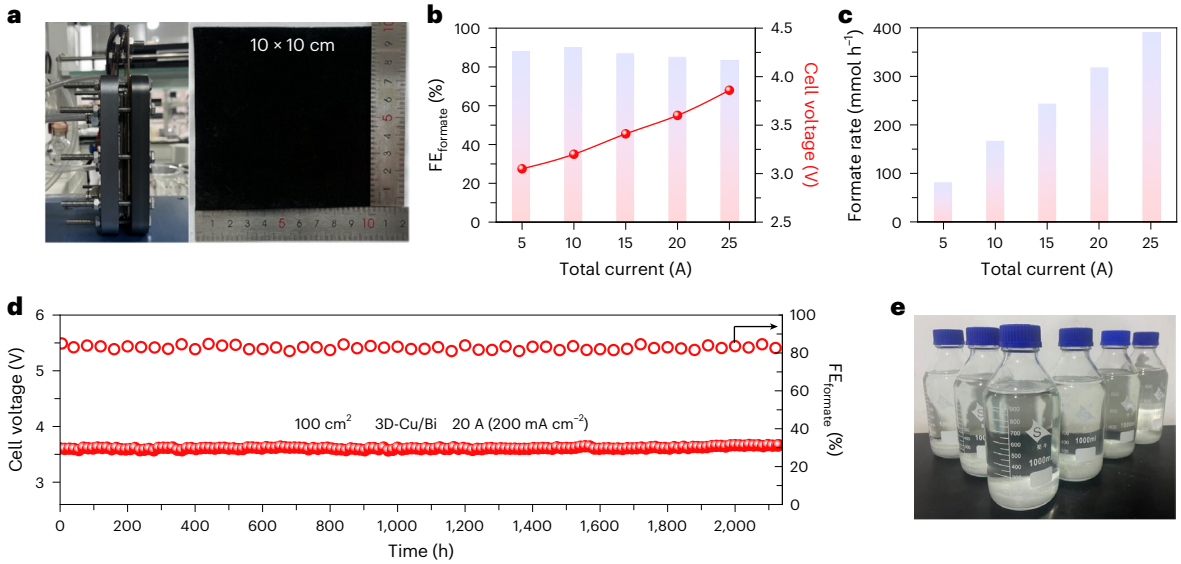

Fig. 5 | Scaled-up demonstration. a, Photographs of the MEA-based CO_2 electrolyser (left) and 3D-Cu/Bi electrode (right) with an area of 100 cm^2. **b**,**c**, Formate FE and cell voltage (**b**) and formate production rate (**c**) at different currents for the 100 cm^2 CO_2 electrolyser using 3D-Cu/Bi as the cathode. **d**, Results of stability testing for the 100 cm^2 CO_2 electrolyser at a current of 20 A (corresponding to 200 mA cm^{-2}). **e**, Photograph of high-concentration formate solution obtained via continuous production. The salt at the bottom of the bottles is a mixture of HCOOK and $KHCO_3$, as a result of the concentration process of product solution at 80 °C.

production rate of 3.3–3.4 mmol h^{-1} and a high formate FE of ~90% during the 100 h test (Fig. 4a,c). By contrast, the formate production rate for the CFP-Cu/Bi electrolyser starts at 1.1 mmol h^{-1} (Fig. 4b,c), which is three times lower than that for the 3D-Cu/Bi-based electrolyser, and arises from the limited permeation of formate solution through the CFP-Cu/Bi electrode. Moreover, CFP-Cu/Bi shows a markedly deteriorated CO_2RR performance after the 100 h stability test, with the formate production rate decreasing from 1.1 to 0.19 mmol h^{-1} and the formate FE decreasing from 68 to 42%. We also studied the effect of the pore size of the catalyst substrate on the formate production rate (Fig. 4d,e and Supplementary Figs. 40–42). The CFP-Cu/Bi with the smallest mean pore size of 35 µm shows the lowest formate production rate. For the Cu foam-based Cu/Bi catalysts, the formate production rate gradually increases along with the increase in the mean pore size from 40 to 120 µm, and reaches a plateau with the mean pore sizes of 190 and 350 µm. The formate production rate of the Cu foam-based catalyst with a 40 µm pore size is close to that of the CFP-Cu/Bi catalyst (Fig. 4e), indicating that the large pore size of the Cu foam (190 µm used in this study) plays a key role in enabling fast migration of the high-concentration formate solution to give the outstanding stability of our electrolyser.

To study the diffusion of CO_2 gas on the 3D-Cu/Bi electrode, we first compared the electrode mass before and after CO_2RR electrolysis and found that the large pores of the Cu foam were not filled by the liquid products (Supplementary Fig. 43). Confocal fluorescence microscopy showed that the red fluorescence emission was only seen on the skeleton of the Cu foam and not in the large pores for the 3D-Cu/Bi electrode after electrolysis (Fig. 4f and Supplementary Fig. 44). We can thus conclude that the large pores of 3D-Cu/Bi were not flooded by liquid during CO_2RR electrolysis. We also used the in situ electrochemical fluorescence spectroscopy method to determine the local CO_2 concentration on the 3D-Cu/Bi and CFP-Cu/Bi surfaces. The local CO_2 concentration of 3D-Cu/Bi is higher than that of CFP-Cu/Bi at the applied current densities (Supplementary Figs. 45 and 46), which could be attributed to the facile diffusion of CO_2 gas to the catalyst surface from the large pores of the 3D-Cu/Bi electrode. However, for the CFP-Cu/Bi electrode, the slow permeation of liquid through the CFP substrate does cause the rapid liquid flooding, thus leading to the low local CO_2 concentration and poor CO_2RR performance.

We then used finite-element analysis to simulate the formate concentration distribution on the surfaces of the 3D-Cu/Bi and CFP-Cu/Bi electrodes. For 3D-Cu/Bi, the formate solution was uniformly distributed with an approximate formate concentration of 4–5 M at different reaction times (Fig. 4g and Supplementary Fig. 47), which is indicative of the stable permeation of formate through this electrode. However, the gradual accumulation of formate solution was observed on CFP-Cu/Bi with the extended reaction time (Fig. 4h and Supplementary Fig. 48), leading to a clear increase in the local formate concentration from ~12 to ~22 M after 100 h of operation. The local formate concentration on the CFP-Cu/Bi surface is even higher than the formate solubility of 15 M in water, which easily causes the formation of formate salt precipitation and subsequent blockage of the CFP-Cu/Bi electrode.

These results were further confirmed by post-catalysis characterization of the two electrodes. The spent 3D-Cu/Bi electrode showed a clean surface with a small amount of salt precipitation after CO_2 electrolysis, which was further verified via cross-sectional SEM elemental mapping and measurement of the residual K^+ content (Supplementary Figs. 49 and 50). In sharp contrast, substantial salt precipitation and a high K^+ residue content were found on the CFP-Cu/Bi electrode (Supplementary Figs. 49 and 50). This could be attributed to the slow permeation of high-concentration formate through the CFP-Cu/Bi electrode, leading to the gradual formation of salt precipitation and thus poor stability. For the 3D-Cu/Bi electrode, its rich macropores provide high-flux channels for fast transport of the liquid product. Overall, the use of the high-flux 3D-Cu/Bi electrode enables the production of highly concentrated formate solution with high stability.

Scaled-up demonstration

To test the practical application of our CO_2RR-to-formate conversion technology, we scaled up the preparation process of the 3D-Cu/Bi electrolyser by increasing the electrode dimensions from 1 cm^2 to 100 cm^2, and then assembled a larger-sized CO_2 electrolyser with an active area of 100 cm^2 to continuously produce concentrated formate solution (Fig. 5a). The uniform Cu/Bi ratios over the whole electrode area and the increased serpentine flow-field channels can enable unaffected mass transfer after scaling up the electrolyser

(Supplementary Figs. 51 and 52). The scaled-up electrolyser still exhibited a high formate FE of ~90% over the wide current range of 5–25 A (corresponding to 50–250 mA cm^{-2}) and a high formate production rate of 390 mmol h^{-1} at 25 A (Fig. 5b,c). This 100 cm^2 electrolyser can achieve excellent stability for over 2,000 h with a formate production rate of 318 mmol h^{-1} at 20 A (Fig. 5d,e and Supplementary Video 2), demonstrating the great potential for the practical application of our high-flux MEA design. We further optimized the anode preparation process of the 100 cm^2 electrolyser to reduce the cell voltage to 2.93 V at 200 mA cm^{-2}, which also showed excellent long-term stability (Supplementary Fig. 53).

Conclusions

In conclusion, we constructed a Cu/Bi heterostructure catalyst on high-flux Cu foam (3D-Cu/Bi), which displays an excellent CO_2RR performance towards the production of formate. Specifically, when operated in an MEA-based CO_2 electrolyser using 3D-Cu/Bi as the cathode fed with dry CO_2 gas and without adding any catholyte, the system can continuously generate 4.5 M formate with a high FE of ~90% for more than 8,000 h at 200 mA cm^{-2}. This performance is very strong in terms of the formate concentration, selectivity and operating time in the context of reported CO_2RR-to-formate electrolysers. We attribute such a performance to the fast migration of concentrated formate through the high-flux 3D-Cu/Bi electrode. We also demonstrate the scalability of our system to a larger-sized electrolyser with an active area of 100 cm^2, which can achieve a high formate production rate of 318 mmol h^{-1} at 20 A for 2,000 h. Such stability represents a remarkable achievement in CO_2 electrolysis and powerfully demonstrates the technological value of our proposed high-flux strategy. This progress provides opportunities in electrocatalytic CO_2 reduction for the generation of liquid products with the simultaneous achievement of high concentration, selectivity and stability, and promotes the development and industrial-scale application of CO_2 electroreduction technology.

Methods

Chemicals and materials

HCl (36%), H_2SO_4 (98%), $(NH_4)_2S_2O_8$ (98%), NaOH (96%), $KHCO_3$ (99.5%), $Bi(NO_3)_3{\cdot}5H_2O$ (99%), K_2SO_4 (99%), commercial Cu powder (99.9%) and commercial Bi powder (99.9%) were purchased from Shanghai Macklin Biochemical Technology Co. The original CFP (TPG-H-60) and MPL-coated CFP (YLS-30T) were purchased from Toray. Cu foam (1 mm thickness) was purchased from Kunshan Jia-yi-sheng Electronics Co., with purity of 99.9% and surface roughness of ~100 nm. Nafion 117 membrane was purchased from DuPont. Commercial IrO_2 catalyst was purchased from Anhui Shengshui Technology Co. All of chemicals and materials were used as received without further treatment.

Preparation of electrodes

First, Cu foam was ultrasonically cleaned in acetone and 1 M HCl to remove any organic pollutant and oxide species. Then a $Cu(OH)_2$ nanowire array on the Cu foam was synthesized via a chemical oxidation process by immersing the Cu foam into a mixed aqueous solution of 0.24 M $(NH_4)_2S_2O_8$ and 6 M NaOH for 30 min at 25 °C. The $Cu(OH)_2$ sample was annealed in a muffle furnace at 200 °C for 2 h in an air atmosphere to yield the black 3D-CuO product. Finally, the 3D-Cu was synthesized via the electrochemical reduction of 3D-CuO at a constant current density of −5 mA cm^{-2} for 100 min in Ar-saturated 0.1 M $KHCO_3$ solution. Bi nanoparticles were coated onto the surface of the 3D-Cu nanowires to form 3D-Cu/Bi using the electrodeposition method with an electrode area of 3 cm^2 at a constant current density of −4 mA cm^{-2} in 20 mM $Bi(NO_3)_3{\cdot}5H_2O$ ethylene glycol solution for 60 min. For comparison, other Cu/Bi samples with Bi deposition times of 20, 40, and 80 min were also prepared. The deposition time was optimized to be 60 min on the basis of the electrocatalytic CO_2RR performance. 3D-Bi was synthesized via the direct deposition of Bi onto the Cu foam substrate.

To synthesize CFP-Cu/Bi, commercial Cu powder as the Cu precursor was coated on the CFP with a Nafion binder. The remaining preparation of CFP-Cu/Bi was same as that for 3D-Cu/Bi except that CFP-Cu powder was used in place of Cu foam as the substrate.

Characterization

X-ray diffraction patterns were recorded using a Rigaku SmartLab 9 kW system equipped with Cu Kα radiation (λ = 1.5418 Å). SEM images were obtained using an FEI Verios 460L scanning electron microscope. Transmission electron microscopy and high-resolution transmission electron microscopy measurements were performed using an FEI Talos F200X transmission electron microscope. The X-ray photoelectron spectra were obtained using a Thermo Scientific ESCALAB250Xi photoelectron spectrometer equipped with an Al Kα (1,486.6 eV) X-ray source. CO_2 adsorption isotherms were recorded at 298 K using a multi-station specific surface micropore and vapour adsorption analyser (MicrotracBEL, BELSORP-Max). In situ ATR-IR spectra were collected using a Fourier transform IR spectrometer (Nicolet iS50, Thermo Scientific) equipped with an MCT-A detector. The spectra were collected at a resolution of 4 cm^{-1}, and each single-beam spectrum was an average of 32 scans. To determine the mean pore size of the CFP and Cu foam samples, mercury intrusion porosimetry was carried out using an AutoPore V9620 (Micromeritics) porosimeter machine. The rhodamine B-labelled electrode was imaged using a confocal fluorescence microscope (A1HD25, Nikon) at an excitation wavelength of 561 nm. The local CO_2 concentration was measured using a fluorescence spectrophotometer (FLS1000, Edinburgh Instruments) using 8-hydroxypyrene-1,3,6-trisulfonic acid as the fluorescent probe molecule[43,44].

Electrochemical measurements in an H-type cell

The CO_2RR performance was assessed in a customized H-type cell with a three-electrode construction controlled by a CHI 760E electrochemical workstation. The 3D-Cu, 3D-Bi and 3D-Cu/Bi catalysts were used directly as the working electrode, Ag/AgCl was the reference electrode and platinum sheet was the counter electrode. CO_2-saturated 0.5 M K_2SO_4 containing different concentrations of H_2SO_4 (0/3/30 mM) was used as the catholyte, and the same solution without CO_2 bubbling was used as the anolyte, and these were separated by a proton exchange membrane (Nafion 117). We first performed linear sweep voltammetry tests for different catalysts at a scan rate of 5 mV s^{-1}. The product FEs were assessed at constant potential, and the gas and liquid products were collected for measurements. Electrochemical impedance spectroscopy measurements were carried out under frequencies ranging from 10^6 Hz to 0.1 Hz with an amplitude of 5 mV at open-circuit voltage.

Electrochemical measurements in an MEA-based CO_2 electrolyser

The MEA-based CO_2 electrolyser consists of a 3D-Cu/Bi or CFP-Cu/Bi electrode as the cathode. The anode was prepared using a catalyst-coated membrane method, where the anodic IrO_2 catalyst and a proton exchange membrane (Nafion 117) were hot-pressed together at 130 °C under a pressure of 5 MPa. Then, the cathode, IrO_2-coated membrane and Ti mesh (the anode current collector) were pressed tightly to form a compact sandwich structure. The anolyte (0.5 M K_2SO_4 plus 3 mM H_2SO_4 solution) was supplied via a peristaltic pump with a unidirectional flow (a 1.5 and 50 ml min^{-1} for the 1 and 100 cm^2 electrolysers, respectively) to prevent any change in K^+ concentration and pH value. We then replenished the K^+ and adjusted the pH of the collected anolyte, which was used to conduct another round to avoid any waste of the anolyte. The cathode was fed with dry CO_2 gas without any catholyte, with CO_2 gas rates of 5 and 300 sccm for the 1 and 100 cm^2 electrolysers, respectively. The product FE and long-term stability were tested at constant current density.

Product analysis

The gas products were analysed using a gas chromatograph (Shimadzu GC-2014) equipped with four columns (a Molsieve 5A, two Porapak N and a Porapak Q) and TCD and FID dual detectors. The liquid product was qualitatively analysed via ^{1}H NMR using a Bruker AVANCE III HD 400 MHz digital NMR instrument with water suppression. For the long-term stability testing of the 1 cm^2 electrolyser, the time interval for each collection was ~80 h, and the volume of formate solution obtained per collection cycle for NMR characterization was 0.7–0.8 ml within 1 h of collection. The CO_2 feed gas could drive the liquid products from the cathode to the outlet without any specific collection apparatus. The collected liquid was first diluted to 40 ml with deionized water and then underwent a second 100-fold dilution. Subsequently, the finally diluted solution (450 µl) was mixed with dimethyl sulfoxide (50 µl) internal standard solution (comprising D_2O (2 ml) and dimethyl sulfoxide (1 µl)) for NMR characterization. For the long-term stability testing of the 100 cm^2 electrolyser, the time interval for each collection was ~40 h, and the volume of formate solution obtained per collection cycle for NMR characterization was 12–13 ml within 10 min of collection.

The Faradaic efficiency of formate ($FE_{formate}$) was calculated using the following equation:

$$FE_{formate}\,(\%) = \frac{2 \times n \times F}{i \times t} \times 100, \quad (1)$$

where n (mol) is the number of moles of formate from the NMR result, F is the Faraday constant (96,485 C mol^{-1}), i (A) is the applied current and t (s) is the electrolysis time.

The formate production rate ($R_{formate}$) was calculated using the following equation:

$$R_{formate}\,(\text{mmol h}^{-1}) = \frac{n}{t}, \quad (2)$$

where n (mmol) is the number of moles of formate (as above) and t (h) is the electrolysis time.

The liquid permeation rate (P_{liquid}) in Fig. 1c,d was calculated using the following equation:

$$P_{liquid}\,(\text{ml s}^{-1}) = \frac{V}{t}, \quad (3)$$

where V (ml) is the volume of permeation liquid from one side of the H-type cell to the other through the electrode and t (s) is the required time.

DFT calculations

All calculations were performed using the Vienna ab initio simulation package[45,46]. The generalized gradient approximation of Perdew–Burke–Ernzerhof[47] functional was adopted for the electron exchange–correlation. The projector augmented-wave method[48] was used to describe the electron–ion interaction. During the calculations, the valence states were expanded in a plane-wave basis set with a cut-off energy of 400 eV, and the Bi(6s6p), Cu(3d, 4s), O(2s2p), C(2s2p) and H(1s) electrons were treated as the valence states.

For Bi(012), the computational model was a periodic slab with a (2 × 3) surface unit cell, which contains six layers and 72 atoms. During the calculations, the top two layers were relaxed and the bottom four layers were frozen, and the Brillouin zone was sampled by a Monkhorst–Pack mesh with a 3 × 3 × 1 grid in reciprocal space. For Cu(111), the computational model was a periodic slab with a (4 × 4) surface unit cell, which contains four layers and 64 atoms. During the calculations, the top two layers were relaxed and the bottom two layers were frozen, and the Brillouin zone was sampled by a Monkhorst–Pack mesh with a 3 × 3 × 1 grid in reciprocal space. For Bi(012)/Cu(111), the computational model was periodic with four layers of Bi(012) and six layers of Cu(111). During the calculations, the top two layers for Bi(012) and three layers for Cu(111) were relaxed, and the Brillouin zone was sampled by a Monkhorst–Pack mesh with a 2 × 2 × 1 grid in reciprocal space. A 15 Å vacuum layer was set for the three computational modelw to avoid any interaction between two adjacent layers. To balance the computational cost and accuracy, the convergence tolerance was set to 10^{-5} eV for energy variation and 0.03 eV Å^{-1} for the force on each atom. In addition, the van der Waals interactions were accounted for using the DFT-D3 method with Becke–Johnson damping[49].

The Gibbs free energy of each intermediate in the simulated pathway was calculated as follows:

$$G = E_{DFT} + E_{ZPE} + \int C_V \mathrm{d}_T - TS, \quad (4)$$

where E_{DFT} is the electronic energy directly obtained from DFT calculations, E_{ZPE} is the zero-point vibrational energy, $\int C_V\,\mathrm{d}T$ is the heat capacity at constant volume, T is the temperature (298.15 K) and S is the entropy.

Finite-element analysis

The models for finite-element analysis were constructed in COMSOL Multiphysics v6.1 as 3D models. The Cu foam with a thickness of 1 mm and a porosity of ~0.9 was used as the model to simplify the simulation. The CFP with a thickness of 180 µm and a porosity of ~0.6 was used as the model to simplify the simulation. For all models, a mesh comprising tetrahedral elements was used, and a linear shape function was used to discretize the computational domain. The 'laminar flow' and 'transport of dilute species' modules were used. For the 'laminar flow' module, the upper boundary was set as the inlet, with a prescribed volumetric flow rate, and the lower boundary was set as the outlet with a static pressure of zero. 'No-slip' walls were set at all of the catalyst–electrolyte interfaces. The lateral boundaries were set as 'symmetry' or 'periodic flow condition'. For the 'transport of dilute species' module, the plane away from the top boundary was set as an 'inflow' boundary with a prescribed time-varying formate anion concentration. The lower boundary was set as an 'outflow' boundary. The lateral boundaries were set as 'symmetry' or 'periodic flow condition'. All of the other boundaries were set as 'no flux'.

For the entire computational domain, the effects of both convective and diffusive mass transport were taken into consideration, whereas the homogeneous reactions involving formate in the electrolyte were neglected. Therefore, the governing equations for transient mass and momentum transport in this specific study read:

$$\frac{\partial c}{\partial t} + \nabla \cdot (c\mathbf{V} - D\nabla c) = 0 \quad (5)$$

$$\nabla \cdot \mathbf{V} = 0 \quad (6)$$

$$\frac{\partial(\rho\mathbf{V})}{\partial t} + \nabla \cdot (\rho\mathbf{V}\mathbf{V}) = -\nabla p + \mu\nabla^2\mathbf{V}, \quad (7)$$

where c is the formate concentration, t is the time, $\mathbf{V}$ is the flow velocity, D is the local diffusivity of formate in the electrolyte (1.45×10^{-9} m^2 s^{-1}), ρ is the density of aqueous electrolyte, p is the static pressure of aqueous electrolyte and μ is the dynamic viscosity of water (8.95×10^{-4} Pa s). For both models, a separated solver was used.

Data availability

All other data are available from the corresponding author upon request. Source data are provided with this paper.

References

1. De Luna, P. et al. What would it take for renewably powered electrosynthesis to displace petrochemical processes? *Science* **364**, eaav3506 (2019).

2. Ozden, A. et al. Carbon-efficient carbon dioxide electrolysers. *Nat. Sustain.* **5**, 563–573 (2022).
3. Fang, W. et al. Durable CO_2 conversion in the proton-exchange membrane system. *Nature* **626**, 86–91 (2024).
4. Jiao, J. et al. Constructing asymmetric double-atomic sites for synergistic catalysis of electrochemical CO_2 reduction. *Nat. Commun.* **14**, 6164 (2023).
5. Rong, X., Wang, H.-J., Lu, X.-L., Si, R. & Lu, T.-B. Control synthesis of vacancy-defect single-atom catalyst for boosting CO_2 electroreduction. *Angew. Chem. Int. Ed.* **59**, 1961–1965 (2020).
6. Wakerley, D. et al. Gas diffusion electrodes, reactor designs and key metrics of low-temperature CO_2 electrolysers. *Nat. Energy* **7**, 130–143 (2022).
7. Kibria, M. G. et al. Electrochemical CO_2 reduction into chemical feedstocks: from mechanistic electrocatalysis models to system design. *Adv. Mater.* **31**, 1807166 (2019).
8. Lv, J.-J. et al. Microenvironment engineering for the electrocatalytic CO_2 reduction rreaction. *Angew. Chem. Int. Ed.* **61**, e202207252 (2022).
9. Jouny, M., Luc, W. & Jiao, F. General techno-economic analysis of CO_2 electrolysis systems. *Ind. Eng. Chem. Res.* **57**, 2165–2177 (2018).
10. Chi, L.-P. et al. Stabilizing indium sulfide for CO_2 electroreduction to formate at high rate by zinc incorporation. *Nat. Commun.* **12**, 5835 (2021).
11. Bushuyev, O. S. et al. What should we make with CO_2 and how can we make it? *Joule* **2**, 825–832 (2018).
12. Wang, W.-H., Himeda, Y., Muckerman, J. T., Manbeck, G. F. & Fujita, E. CO_2 hydrogenation to formate and methanol as an alternative to photo- and electrochemical CO_2 reduction. *Chem. Rev.* **115**, 12936–12973 (2015).
13. Álvarez, A. et al. Challenges in the greener production of formates/formic acid, methanol, and DME by heterogeneously catalyzed CO_2 hydrogenation processes. *Chem. Rev.* **117**, 9804–9838 (2017).
14. Zheng, T. et al. Copper-catalysed exclusive CO_2 to pure formic acid conversion via single-atom alloying. *Nat. Nanotechnol.* **16**, 1386–1393 (2021).
15. Fan, L., Xia, C., Zhu, P., Lu, Y. & Wang, H. Electrochemical CO_2 reduction to high-concentration pure formic acid solutions in an all-solid-state reactor. *Nat. Commun.* **11**, 3633 (2020).
16. Xia, C. et al. Continuous production of pure liquid fuel solutions via electrocatalytic CO_2 reduction using solid-electrolyte devices. *Nat. Energy* **4**, 776–785 (2019).
17. Zhu, P. & Wang, H. High-purity and high-concentration liquid fuels through CO_2 electroreduction. *Nat. Catal.* **4**, 943–951 (2021).
18. Wang, Z. et al. Carbon-confined indium oxides for efficient carbon dioxide reduction in a solid-state electrolyte flow cell. *Angew. Chem. Int. Ed.* **61**, e202200552 (2022).
19. Fernández-Caso, K., Díaz-Sainz, G., Alvarez-Guerra, M. & Irabien, A. Electroreduction of CO_2: advances in the continuous production of formic acid and formate. *ACS Energy Lett.* **8**, 1992–2024 (2023).
20. Yang, H., Kaczur, J. J., Sajjad, S. D. & Masel, R. I. Performance and long-term stability of CO_2 conversion to formic acid using a three-compartment electrolyzer design. *J.CO2 Util.* **42**, 101349 (2020).
21. Zhang, Z. et al. Membrane electrode assembly for electrocatalytic CO_2 reduction: principle and application. *Angew. Chem. Int. Ed.* **62**, e202302789 (2023).
22. Ge, L. et al. Electrochemical CO_2 reduction in membrane-electrode assemblies. *Chem* **8**, 663–692 (2022).
23. Wang, Z. et al. Efficient electroconversion of carbon dioxide to formate by a reconstructed amino-functionalized indium–organic framework electrocatalyst. *Angew. Chem. Int. Ed.* **60**, 19107–19112 (2021).
24. Li, W. et al. Bifunctional ionomers for efficient co-electrolysis of CO_2 and pure water towards ethylene production at industrial-scale current densities. *Nat. Energy* **7**, 835–843 (2022).
25. Wonhee, L., Eun, K. Y., Hye, Y. M., Kwan, J. S. & Tae, P. K. Catholyte-free electrocatalytic CO_2 reduction to formate. *Angew. Chem. Int. Ed.* **57**, 6883–6887 (2018).
26. Li, L. et al. Stable, active CO_2 reduction to formate via redox-modulated stabilization of active sites. *Nat. Commun.* **12**, 5223 (2021).
27. Bi, J. et al. High-rate CO_2 electrolysis to formic acid over a wide potential window: an electrocatalyst comprised of indium nanoparticles on chitosan-derived graphene. *Angew. Chem. Int. Ed.* **62**, e202307612 (2023).
28. Abdinejad, M. et al. Insertion of MXene-based materials into Cu–Pd 3D aerogels for electroreduction of CO_2 to formate. *Adv. Energy Mater.* **13**, 2300402 (2023).
29. Wan, Y. et al. Oxidation state modulation of bismuth for efficient electrocatalytic nitrogen reduction to ammonia. *Adv. Funct. Mater.* **31**, 2100300 (2021).
30. Li, Z. et al. Electron-rich Bi nanosheets promote $CO_2^{\cdot-}$ formation for high-performance and pH-universal electrocatalytic CO_2 reduction. *Angew. Chem. Int. Ed.* **62**, e202217569 (2023).
31. Huang, J. E. et al. CO_2 electrolysis to multicarbon products in strong acid. *Science* **372**, 1074–1078 (2021).
32. Chi, L.-P. et al. Efficient and stable acidic CO_2 electrolysis to formic acid by a reservoir structure design. *Proc. Natl Acad. Sci. USA* **120**, e2312876120 (2023).
33. Li, Y. et al. Coupling CO_2 reduction with CH_3OH oxidation for efficient electrosynthesis of formate on hierarchical bifunctional CuSn alloy. *Nano Energy* **98**, 107277 (2022).
34. Tang, J. et al. Advantages of eutectic alloys for creating catalysts in the realm of nanotechnology-enabled metallurgy. *Nat. Commun.* **10**, 4645 (2019).
35. Jia, G. et al. Size effects of highly dispersed bismuth nanoparticles on electrocatalytic reduction of carbon dioxide to formic acid. *J. Am. Chem. Soc.* **145**, 14133–14142 (2023).
36. Duan, Y.-X. et al. Boosting production of HCOOH from CO_2 electroreduction via Bi/CeO_x. *Angew. Chem. Int. Ed.* **60**, 8798–8802 (2021).
37. Fan, J. et al. Large-area vertically aligned bismuthene nanosheet arrays from galvanic replacement reaction for efficient electrochemical CO_2 conversion. *Adv. Mater.* **33**, 2100910 (2021).
38. Xue, H., Zhao, Z.-H., Liao, P.-Q. & Chen, X.-M. "Ship-in-a-bottle" integration of ditin(IV) sites into a metal–organic framework for boosting electroreduction of CO_2 in acidic electrolyte. *J. Am. Chem. Soc.* **145**, 16978–16982 (2023).
39. Liang, S. et al. Sulfur changes the electrochemical CO_2 reduction pathway over Cu electrocatalysts. *Angew. Chem. Int. Ed.* **62**, e202310740 (2023).
40. Wang, T. et al. Halogen-incorporated Sn catalysts for selective electrochemical CO_2 reduction to formate. *Angew. Chem. Int. Ed.* **62**, e202211174 (2023).
41. Lin, L. et al. A nanocomposite of bismuth clusters and $Bi_2O_2CO_3$ sheets for highly efficient electrocatalytic reduction of CO_2 to formate. *Angew. Chem. Int. Ed.* **62**, e202214959 (2023).
42. Lv, L. et al. Coordinating the edge defects of bismuth with sulfur for enhanced CO_2 electroreduction to formate. *Angew. Chem. Int. Ed.* **62**, e202303117 (2023).
43. Geng, Q. et al. Revolutionizing CO_2 electrolysis: fluent gas transportation within hydrophobic porous Cu_2O. *J. Am. Chem. Soc.* **146**, 10599–10607 (2024).
44. Shi, R. et al. Efficient wettability-controlled electroreduction of CO_2 to CO at Au/C interfaces. *Nat. Commun.* **11**, 3028 (2020).
45. Kresse, G. & Hafner, J. Ab initio molecular-dynamics simulation of the liquid-metal–amorphous-semiconductor transition in germanium. *Phys. Rev. B* **49**, 14251–14269 (1994).

46. Kresse, G. & Furthmüller, J. Efficient iterative schemes for ab initio total-energy calculations using a plane-wave basis set. *Phys. Rev. B* **54**, 11169–11186 (1996).
47. Perdew, J. P., Burke, K. & Ernzerhof, M. Generalized gradient approximation made simple. *Phys. Rev. Lett.* **77**, 3865–3868 (1996).
48. Blöchl, P. E. Projector augmented-wave method. *Phys. Rev. B* **50**, 17953–17979 (1994).
49. Grimme, S., Antony, J., Ehrlich, S. & Krieg, H. A consistent and accurate ab initio parametrization of density functional dispersion correction (DFT-D) for the 94 elements H–Pu. *J. Chem, Phys.* **132**, 154104 (2010).

Acknowledgements

This work was supported by the National Key R&D Program of China (2022YFA1502902 to T.-B.L.) and the National Natural Science Foundation of China (22531007 to T.-B.L. and 22375146 to Z.-Y.Y.).

Author contributions

Z.-Y.Y. and T.-B.L. conceived and designed the project. J.-J.L. performed the experiments, collected and analysed the data. H.-J.W. carried out the DFT calculationS. C.Z. performed the finite-element analysis. Y.L., J.J., L.-L.W., C.W., D.-C.Z. and Z.-Y.W. helped with analysing the results. J.-J.L., Z.-Y.Y. and T.-B.L. wrote and revised the paper.

Competing interests

The authors declare no competing interests.

Additional information

Supplementary information The online version contains supplementary material available at https://doi.org/10.1038/s41929-026-01524-9.

Correspondence and requests for materials should be addressed to Zi-You Yu or Tong-Bu Lu.

Peer review information *Nature Catalysis* thanks Lei Wang and the other, anonymous, reviewer(s) for their contribution to the peer review of this work.